International Journal of Mechanical, Industrial and Aerospace Sciences
ISSN: 2517-9950
Vol:13, No:9, 2019

Evaluation of the Power Generation Effect Obtained by Inserting a Piezoelectric Sheet in the Backlash Clearance of a Circular Arc Helical Gear

Barenten Suciu, Yuya Nakamoto

***Abstract*—**Power generation effect, obtained by inserting a piezo-electric sheet in the backlash clearance of a circular arc helical gear, is evaluated. Such type of screw gear is preferred since, in comparison with the involute tooth profile, the circular arc profile leads to reduced stress-concentration effects, and improved life of the piezoelectric film. Firstly, geometry of the circular arc helical gear, and properties of the piezoelectric sheet are presented. Then, description of the test-rig, consisted of a right-hand thread gear meshing with a left-hand thread gear, and the voltage measurement procedure are given. After creating the tridimensional (3D) model of the meshing gears in SolidWorks, they are 3D-printed in acrylonitrile butadiene styrene (ABS) resin. Variation of the generated voltage versus time, during a meshing cycle of the circular arc helical gear, is measured for various values of the center distance. Then, the change of the maximal, minimal, and peak-to-peak voltage versus the center distance is illustrated. Optimal center distance of the gear, to achieve voltage maximization, is found and its significance is discussed. Such results prove that the contact pressure of the meshing gears can be measured, and also, the electrical power can be generated by employing the proposed technique.

***Keywords*—**Power generation, circular arc helical gear, piezo-electric sheet, contact problem, optimal center distance.

I. Introduction

MEASUREMENT of the contact pressure distribution on the flank of the meshing gears is very important in order to validate the contact pressure computations, and in order to understand the causes of the gear damage [1]-[3]. Moreover, the influence of the geometrical and stiffness alterations, due to the sensor presence, should be negligible in order to achieve a reliable measurement method of the contact pressure [1]-[3].

Several measurement techniques are well-known in the literature, such as the physical or chemical deposition of thin film sensors, with a thickness of a few micrometers, on the gear flank [1]-[3], the insertion of the so-called prescale pressure measurement films in the gear backlash [4], etc. For instance, the pressure measurement films are usable form the minimal pressure of 0.006 MPa, up to the maximal pressure of 300 MPa [4]. According to the desired measuring range, they can be selected in the following pressure intervals: 0.006-0.05 MPa, 0.05-0.2 MPa, 0.2-0.5 MPa, 0.5-2.5 MPa, 2.5-10 MPa, 10-50 MPa, 50-130 MPa, and 130-300 MPa [4]. Such measurement films are consisted of two polyester sheets, one sheet being coated by a layer of micro-encapsulated color forming material, and the other by a layer of color developing material [4]. Microcapsules are designed to break at a certain pressure that corresponds to a specific color density. By using charts that correlate the pressure and the color density, the effective contact pressure can be accurately determined, after applying corrections for the environmental temperature and humidity [4]. Although the measurement films are relatively cheap and reliable, they are unable to record the variation of the contact pressure versus time, but merely the maximal pressure distribution occurring on the flank of the meshing gears [3]. On the other hand, although costly and suitable only for higher pressures, ranging from 10 to 1,000 MPa, the thin film sensors can be employed to measure the dynamically varying pressures, occurring either in dry solid-solid contacts, or even in the thin lubricant pellicle present between meshing teeth [3].

In this work, instead of the traditional involute tooth profile, used for spur [1] and helical [3] gears, a circular arc profile, cut as a spiral thread in order to achieve a helical gear [5]-[12], is considered. This kind of circular arc helical gear is preferable since the stress-concentration is virtually nonexistent [6]. Then, instead of a pressure measurement film, or a thin film sensor, a piezoelectric sheet [13] is inserted in the backlash clearance between the meshing gears, as a relatively cheap alternative to measure the dynamically varying lower pressures. Proposed technique is based on the fact that a dynamical voltage occurs between the terminals of the piezoelectric sheet when the meshing gears are rotated.

Note that, quite a large variety of applications are envisaged for the piezoelectric sheets, such as acceleration, vibration, and motion sensors, switches, acoustic and ultrasonic sensors, etc. [13]. According to the present work, the power generation effect can be added to the list of potential applications, under the reasonable assumption that, a sufficiently long life of the piezoelectric sheet can be expected in the absence of the stress-concentration effects in circular arc helical gears.

II. Geometry of the Circular Arc Helical Gear

Circular arc helical gears are employed in construction of parallel axis transmissions [5]-[7], gear pumps [8], nutation drive mechanisms [9], screw compressors [10], roots blowers [11], [12], etc. In comparison with the spur type rotors, in the case of helical rotors for pumps, compressors and blowers, 2-4 lobes are twisted in a spiral shape. As a result, the helical rotors

Barenten Suciu is with the Department of Intelligent Mechanical Engineering, Fukuoka Institute of Technology, Fukuoka, 811-0295 Japan (corresponding author, phone: +81-92-606-4348; fax: +81-92-606-0747; e-mail: suciu@fit.ac.jp).

Yuya Nakamoto is with the Department of Intelligent Mechanical Engineering, Fukuoka Institute of Technology, Japan (e-mail: 15e2048@bene.fit.ac.jp)

are able to displace the fluid continuously at a higher rate than the spur type rotors, and are able to prevent the pulsating noise from occurring [10]-[12].

In the first design step of the circular arc helical gears, one should decide the appropriate gear geometry. Majority of the previously reported works, based on relatively complex matrix models, are dealing with aspects concerning the reduction or amplification ratio, meshing conditions, slip ratio, contact ratio, etc. [5]-[11]. However, the equations necessary to calculate the geometrical parameters, such as the diameters of the pitch, tip, root, and rolling circles are omitted, or scarcely listed, without arguing on the grounds for their correctness.

In this work, one observes that the circular arc helical gears and the traditional involute arc helical gears are similar from a geometrical standpoint. For this reason, one generalizes the equations, accepted for involute arc helical gears, by various handbooks [14], and industrial standards [15], and applies them to the case of circular arc helical gears, as follows.

Some geometrical parameters, such as the number of teeth $z = 6$, normal module $m_n = 6$ mm, twist angle $\beta = 39.268$ deg, face-width $b = 60$ mm, and the real center distance $a = 45$, 46, 47, 48, 49, 50 mm of the gear were selected according to the design guidelines provided by [14], [15] (see Table I). The remaining geometrical parameters of the designed circular arc helical gears were calculated by using the following equations, and the obtained numerical values are listed in Table I.

Frontal module, m_t:

$$m_t = m_n / \cos\beta \tag{1}$$

Axial module, m_x:

$$m_x = m_n / \sin\beta \tag{2}$$

Normal pitch, p_n:

$$p_n = \pi \times m_n \tag{3}$$

Frontal pitch, p_t:

$$p_t = \pi \times m_t \tag{4}$$

Axial pitch, p_x:

$$p_x = \pi \times m_x \tag{5}$$

Lead, L:

$$L = z \times p_x \tag{6}$$

Diameter of the pitch circle, d:

$$d = z \times m_t \tag{7}$$

Addendum, h_a:

$$h_a = m_n \tag{8}$$

Diameter of the tip (cap) circle, d_a:

$$d_a = d + 2h_a \tag{9}$$

Dedendum, h_f:

$$h_f = 1.25 m_n \tag{10}$$

Diameter of the root (foot) circle, d_f:

$$d_f = d - 2h_f \tag{11}$$

Contact ratio, ε:

$$\varepsilon = \frac{b}{p_x} = \frac{b}{\pi m_n} \sin\beta \tag{12}$$

Frontal angle of twist, γ:

$$\gamma = 360 \frac{b}{L} \text{ [deg]} \tag{13}$$

Standard distance between the center axes, a_0:

$$a_0 = d \tag{14}$$

Diameter of the rolling circle, d_w:

$$d_w = a \tag{15}$$

Radius of the circular arc root (foot), ρ_f:

$$\rho_f \cong p_t / 4 \tag{16}$$

Radius of the circular arc tip (cap), ρ_a:

$$\rho_a = \rho_f \frac{h_a}{h_f} \tag{17}$$

Fig. 1 shows the face-width b, the angle of twist β, and the frontal angle of twist γ of the designed circular arc helical gear. Next, Fig. 2 illustrates the frontal pitch p_t, diameter of the pitch circle d, diameter of the tip (cap) circle d_a, diameter of the root (foot) circle d_f, addendum h_a, dedendum h_f, radius of the circular arc tip (cap) ρ_a, and the radius of the circular arc root (foot) ρ_f.

TABLE I
GEOMETRICAL PARAMETERS OF THE DESIGNED CIRCULAR ARC HELICAL GEAR

Denomination of the geometrical parameter	Numerical value
Number of teeth	6
Normal module (selected based on JIS B1701 [15])	6 mm
Twist angle	39.268 deg
Frontal module	7.750 mm
Axial module	9.479 mm
Normal pitch	18.850 mm
Frontal pitch	24.347 mm
Axial pitch	29.781 mm
Lead	178.686 mm
Diameter of the pitch circle	46.500 mm
Addendum	6.000 mm
Diameter of the tip (cap) circle	58.500 mm
Dedendum	7.500 mm
Diameter of the root (foot) circle	31.500 mm
Face-width	60 mm
Contact ratio	2.015
Frontal angle of twist	120.882 deg
Standard distance between the center axes	46.500
Real distance between the center axes	45, 46, …, 50 mm
Diameter of the rolling circle	45, 46, …, 50 mm
Radius of the circular arc root (foot)	6.087 mm
Radius of the circular arc tip (cap)	4.869 mm

In order to illustrate the importance of the twist angle β, a comparison of the circular helical gears with nonzero and nil twist angles is presented in Fig. 3. In the case of involute profile spur gears, the overlapping coefficient, or the so-called contact ratio, is commonly larger than 1 but smaller than 2. This means that during the process of power transmission, involute spur gear has always more than one pair of teeth engaged, and hence, the continuous meshing condition is intrinsically guaranteed. Oppositely, in the case of circular profile spur gears of nil twist angle ($\beta = 0$), shown in Fig. 3, the condition of continuous meshing is not satisfied. Indeed, there is only a short period of contact on the tip of the gear. This feature can be also observed from (12), which leads to nil contact ratio ($\varepsilon = 0$) for $\beta = 0$. Lack of continuous meshing for circular arc spur gears is not convenient in applications. Hence, to guarantee the continuous meshing, circular arc gears must be made with oblique teeth.

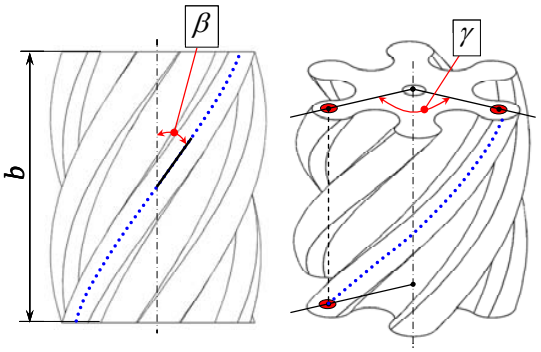

Fig. 1 Geometry of the circular arc helical gear, showing the face-width, the angle of twist, and the frontal angle of twist

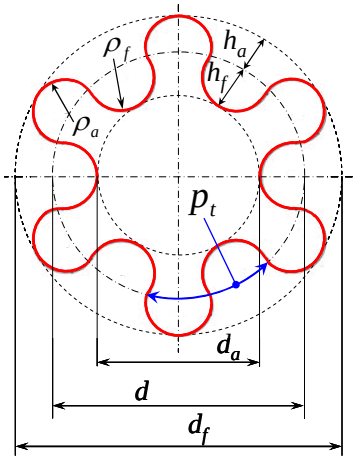

Fig. 2 Geometry of the circular arc helical gear, illustrating the frontal pitch, diameter of the pitch circle, diameter of the tip (cap) circle, diameter of the root (foot) circle, addendum, dedendum, radius of the circular arc tip (cap), and radius of the circular arc root (foot)

Angle of the spiral thread or helix, relative to the axis of symmetry of the gear, is called the twist angle (see Fig. 1). Here, in order to exceed the minimal allowable contact ratio ($\varepsilon > 1$), but in order to achieve the same optimal contact ratio ($\varepsilon \cong 2$) as the involute profile spur gears, the twist angle was selected as $\beta = 39.268$ deg in correlation with b and m_n (see Table I).

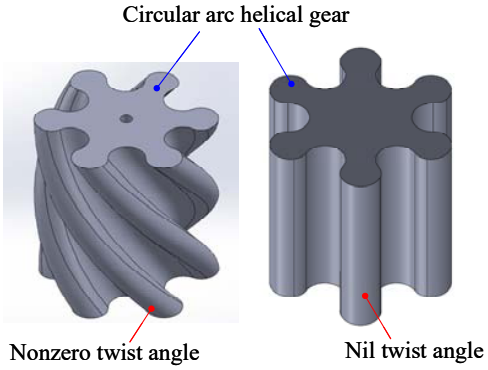

Fig. 3 Comparison of the circular helical gears with nonzero and nil twist angles

III. SPECIFICATIONS OF THE EMPLOYED PIEZOELECTRIC FILM

Ceramic piezoelectric materials, such as barium titanate and lead zirconate titanate, are nowadays largely used for actuation, harvesting, and power generation [16]. Unfortunately, ceramics being brittle materials without malleability, cannot endure large deformations, as required in the proposed application. For this reason, in the present work, a soft polymer-based piezoelectric material, denoted as poly(vinylidene fluoride), and abbreviated as PVDF, is employed. PVDF is consisted from interconnected alkyl chains composed from CH_2 groups and fluorocarbon chains constituted from CF_2 groups [17]-[19]. When a tensile stress is applied in longitudinal and/or width direction of the piezoelectric sheet, the fluorocarbon groups become negatively

charged, and the alky groups positively charged. In this manner a piezoelectric effect can be achieved, even under shocks and large deformations [13], [17]-[19].

Components and dimensions of the piezoelectric sheet, used in this work, are presented in Fig. 4. Thus, the PVDF part of the piezoelectric sheet, having a length of 156 mm, a width of 19 mm, and a thickness of 0.052 mm, is covered for protection on both sides by acrylic coatings of 171 mm length, and 22 mm width. In this way, the total thickness of the piezoelectric sheet becomes 0.064 mm. The necessary conducting wires are firmly connected via rivets to the piezoelectric element. Main features of this piezoelectric sheet can be listed as follows: density of 1780 kg/m^3, tensile strength in longitudinal (width) direction of 140-210 (30-55) MPa, Young modulus of elasticity of 2-4 GPa, rupture strain in longitudinal (width) direction of 2-4% (2-5%), specific dielectric constant of 12, electromechanical constant of 0.12, and piezoelectric output constant of 0.216V·m/N. Next, Fig. 5 shows the attaching method of the piezoelectric sheet to the circular arc helical gear, along the normal direction to the teeth.

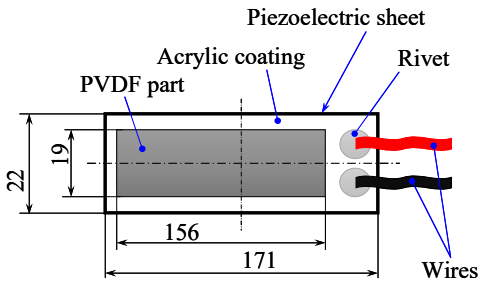

Fig. 4 Components and dimensions of the piezoelectric sheet

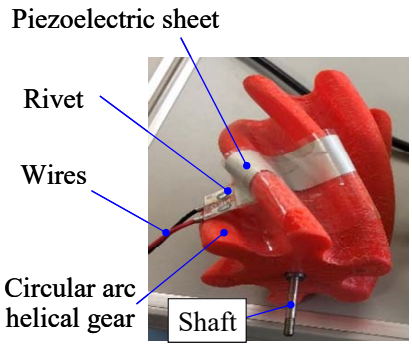

Fig. 5 Attachment of the piezoelectric sheet to the circular arc helical gear, along the normal direction to the teeth

IV. Test-rig and Measurement Procedure

Fig. 6 shows the tridimensional model of the meshing gears, created in SolidWorks, and Fig. 7 presents a photograph of the gear assembly, after printing in ABS resin. With the purpose to achieve proper meshing conditions, a right-hand thread gear, engaging a left-hand thread gear of the same twist angle, was designed and printed.

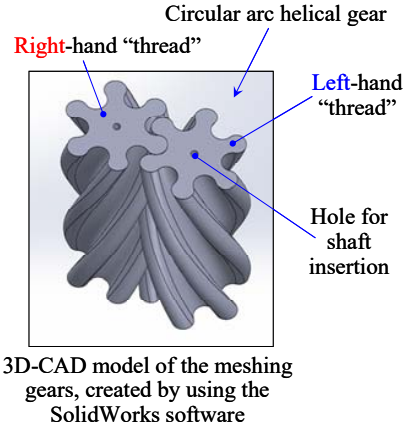

Fig. 6 Tridimensional model of the meshing gears, created in SolidWorks

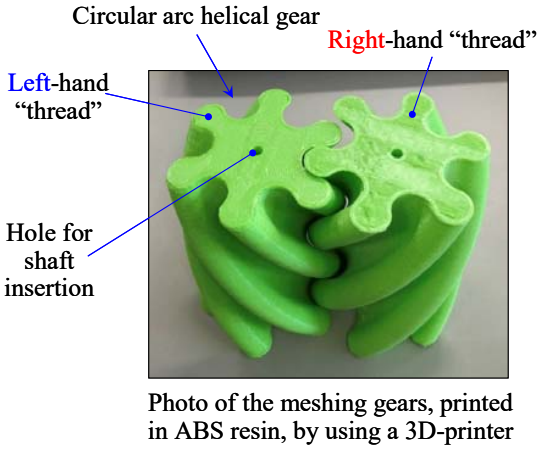

Fig. 7 Photo of the meshing gears, 3D-printed in ABS resin

In order to assemble the counterpart gears on the test rig, press-fitted shafts, inserted in holes of 6 mm diameter, opened along the axes of the circular arc helical gears, were employed. Thus, Fig. 8 illustrates the shape and dimensions of the shaft used to mount the gear on the test-rig. Supplementary, Fig. 9 shows a photograph of the gear, after the shaft was press-fitted into the central hole, opened along the axis of symmetry. Metric threads M3, having a length of 5 mm, are provided at the both ends of the shaft, in order to attach the gear assembly on the test-rig shown by Fig. 10.

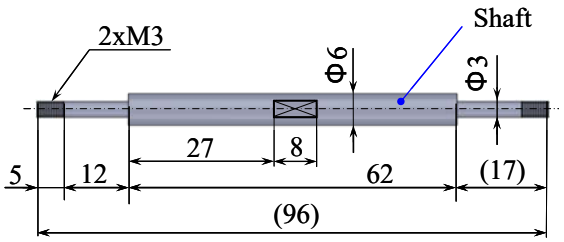

Fig. 8 Drawing of the shaft used to mount the gear on the test-rig

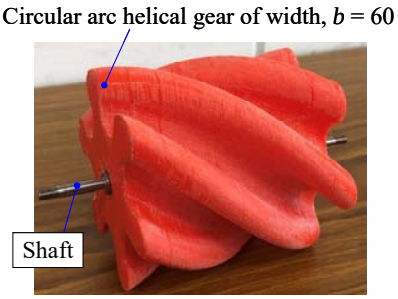

Fig. 9 Photo of the gear, after the shaft was press-fitted into the central hole opened along the axis of symmetry

Fig. 10 shows the test-rig consisted of a base, made in U-type profile, on which two supports are vertically fixed by using M4-type bolts. Two M8 screwed bars are vertically fastened to these supports, by inserting them into the threaded holes of the supports, and by securing them against looseness with nuts. L-type metal fittings are attached to the screwed bars at suitable positions, by using nuts and counter-nuts.

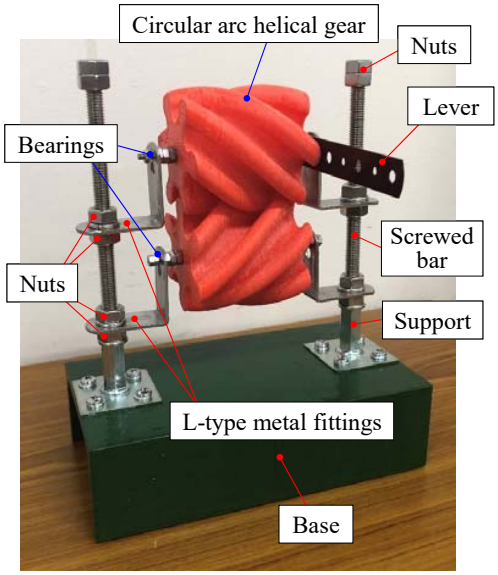

Fig. 10 Photograph of the test-rig showing its main components

L-type metal fittings are furnished with sliding bearings, having sleeves of 3 mm inner diameter, necessary to hold up horizontally the shafts, used to bear the helical gear. By suitably selecting the positions of the L-type metal fittings on the screwed bars, it becomes possible to adjust the real distance between the center axes of the gears, at the values given by Table I, i.e., $a = 45$, 46, 47, 48, 49, and 50 mm.

In order to achieve swinging tests at a maximal rotation angle of 180 deg of the helical gear, a lever is provided to the upper right-hand thread gear (see Figs. 10 and 11). Such arm is rigidly fixed to the upper gear by using the shaft end and a protrusion, fitted into the holes of the lever. Fig. 11 presents the protrusion of 5 mm diameter, and 3 mm height, eccentrically placed on the gear face, at a 12 mm distance from the axis of symmetry.

Fig. 12 illustrates the mobile recorder [20] used to measure the voltage occurring between wires of the piezoelectric sheet, generated when the sheet is squeezed between helical gears.

After recording the experimental data, i.e., variation of the generated voltage versus time, the mobile recorder is connected to a computer for saving and further analysis of the results.

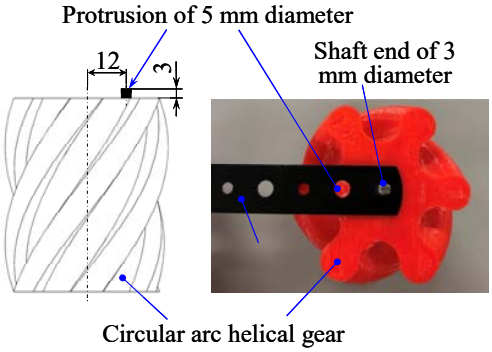

Fig. 11 Geometry of the protrusion used together with the shaft end to attach the lever to the circular helical gear

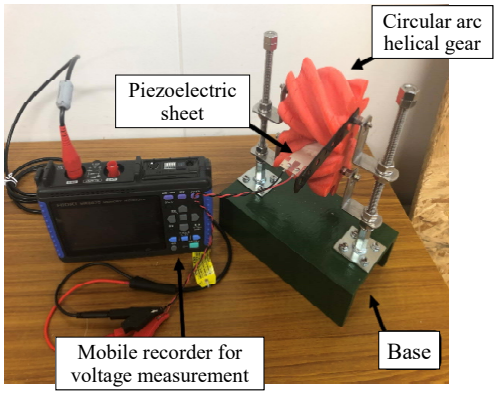

Fig. 12 Photograph showing the mobile recorder used to measure the voltage occurring between the wires of the piezoelectric sheet, generated when the sheet is squeezed between gears

V. Results and Discussions

Fig. 13 presents the variation of the generated voltage versus time during a meshing cycle of the circular arc helical gear, i.e., during swinging tests at a maximal rotation angle of 180 deg. Measurements were performed for various values of the real distance between the center axes of the gear, i.e., $a = 45$ mm (see the results in light green), $a = 46$ mm (see the green solid line), $a = 47$ mm (see the wavy results in red), $a = 48$ mm (see the black solid line), $a = 49$ mm (see the blue solid line), and $a = 50$ mm (see the results in light blue).

As already stressed, the voltage recorded between the wires of the piezoelectric sheet is generated by the tensile stress occurring in longitudinal and/or width direction of the sheet, due to the oppositely charged alkyl and fluorocarbon groups. In conclusion, the wavy variation of the voltage, shown by Fig. 13, appears when the piezoelectric sheet is sandwiched between the tip and the root of the engaging gears, and also when piezo-

electric sheet is squeezed between the flanks of the meshing gears. Due to the thread-like shape of the teeth, tridimensional bending of the PVDF produces tensile stresses both along the longitudinal and width directions of the piezoelectric sheet.

In order to further analyze the nature of the random wavy results shown by Fig. 13, we represent the variation of the maximal voltage U_{max}, minimal voltage U_{min}, and peak-to-peak voltage U_{p-p} against the real distance a between the center axes of the gear (see Fig. 14).

One can observe that the graphs of the peak-to-peak voltage and of the maximal voltage display a mountain-like shape, with apexes ($U_{max,max} = 0.6$ V, $U_{p-p,max} = 1.1$ V) which correspond to an optimal center distance, situated near $a = 48$ mm. On the other hand, the minimal voltage monotonically increases versus the center distance, but the graph shows a mild inflexion point in the vicinity of $a = 48$ mm (see Fig. 14).

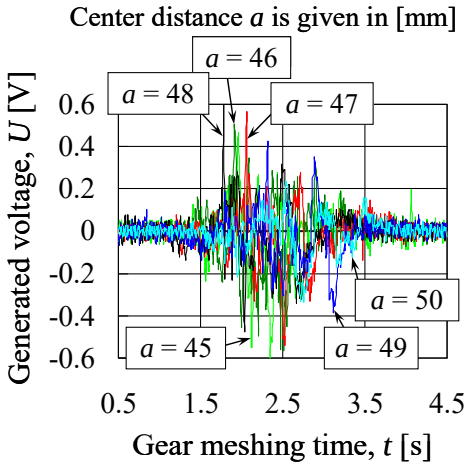

Fig. 13 Variation of the generated voltage versus time during a meshing cycle of the circular arc helical gear, measured for various values of the distance between the center axes of the gear

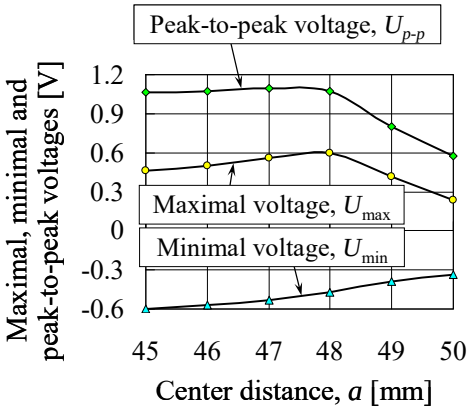

Fig. 14 Variation of the maximal, minimal and peak-to-peak voltages versus the real distance measured between the center axes of the gear

In order to fully explain the phenomenology connected to Figs. 13 and 14, it is indispensable to conceive quite complex models [21], [22]. However, for the sake of simplicity, it can be inferred that the meshing and contact conditions are changing when the real center distance of the gear increases from 45 to 50 mm. Thus, *for short center distances of 45-46 mm*, since the piezoelectric sheet is sandwiched over a larger contact surface, presumably the contact pressures on the teeth, and the bending stresses on the PVDF are smaller, leading to relatively lower values of the peak-to-peak voltage. On the other hand, *for middle center distances of 47-48 mm*, since the piezoelectric sheet appears as squeezed over a smaller contact surface, the contact pressures on the teeth, and the bending stresses on the PVDF are higher, leading to maximization of the peak-to-peak voltage. Finally, *for long center distances of 49-50 mm*, the gears are almost unengaged, i.e., the meshing occurs only on the tips of the teeth, this leading to abrupt decreasing of the peak-to-peak voltage.

Results presented in Figs. 13 and 14 prove that, by inserting a piezoelectric sheet in the backlash clearance of a circular arc helical gear, power generation effect can be achieved. Besides, the optimal distance between the center axes of the gear can be found to maximize the generated voltage. Accordingly, on one hand, it seems that the dynamic contact pressures occurring on the teeth, as well as the corresponding bending stresses occurring on the piezoelectric sheet, can be measured, and, on the other hand, it appears that electrical power can be produced by using the proposed technique.

VI. Conclusions

In this paper, as alternative to the rigid ceramic piezoelectric films, a soft polymer-based piezoelectric sheet made in PVDF, and, as alternative to the traditional involute arc helical gears of higher stress-concentration effects, circular arc helical gears of lower stress-concentration effects, were selected and combined to propose a measuring technique for the contact pressures occurring on the teeth during the meshing process of the gears. This technique appears as a relatively cheap alternative to measure the dynamically varying lower contact pressures of non-metallic gears, but it can be also employed for electric power generation, under eventual refining, aimed to maximize the output of such kind of system.

References

[1] H. Winter, B.R. Hohn, K. Michaelis, and E. Kagerer, "Measurement of Pressure, Temperature and Film Thickness in Disk and Gear Contact," *Proceedings of the JSME International Conference on Motion and Power Transmissions*, pp. 474–479, 1991.

[2] E. Kagerer, and M. Koniger, "Ion Beam Sputter Deposition of Thin Film Sensors for Applications in Highly Loaded Contacts," *Thin Solid Films*, 182, pp. 333–344, 1989.

[3] M. Owashi, and Y. Mihara, "Development of a Measurement Method of Contact Pressure between Gear Teeth Using a Thin-Film Sensor (Measurement of Pressure Distribution by Multi-Point Pressure Sensor with Shared Lead Films)," *Transactions of the JSME C*, 77(782), pp. 3938–3950, 2011 (in Japanese).

[4] "Prescale Pressure Measurement Film," *Fuji Film Instruction Manual*, pp. 1–10, 2018.

[5] Z. Chen, H. Ding, B. Li, L. Luo, L. Zhang, and J. Yang, "Geometry and Parameter Design of Novel Circular Arc Helical Gears for Parallel-axis Transmission," *Advances in Mechanical Engineering*, 9(2), pp. 1–11, 2017.

[6] D. Liang, B. Chen, Y. Gao, S. Peng, and S. Qin, "Geometric and Meshing

Properties of Conjugate Curves for Gear Transmission," *Mathematical Problems in Engineering*, 2014, pp. 484802.1–12, 2014.
[7] Y. Chen, and L. Yao, "Design Formulae for a Concave Convex Arc Line Gear Mechanism," *Mechanical Sciences*, 7, pp. 209–218, 2016.
[8] G. Li, L. Zhang, and W. Han, "Profile Design and Displacement Analysis of the Low Pulsating Gear Pump," *Advances in Mechanical Engineering*, 10(3), pp. 1–11, 2018.
[9] J. Hong, L. Yao, W. Ji, and Z. Huang, "Kinematic Modeling for the Nutation Drive based on Screw Theory," *Proceedings of the 25th Design Conference Innovative Product Creation*, 36, pp. 123–128, 2015.
[10] Y.R. Wu, and Z.H. Fong, "Rotor Profile Design for the Twin-screw Compressor based on the Normal-rack Generation Method," *ASME Journal of Mechanical Design*, 130, pp. 042601.1–8, 2008.
[11] Y. Cai, and L. Yao, "Comparison Analysis and Verification on Spur and Helical Three-lobe Rotors with Novel Tooth Profile in Roots Blower," *Proceedings of the 2nd International Conference on Mechanical, Electronic and Information Technology Engineering*, pp. 418–419, 2016.
[12] "Helical Rotor Blower. Roots Type: ARH-S/SP, AR-E/EP Series," *ShinMaywa General Catalog*, K-3236P, pp. 1–39, 2018.
[13] "Piezoelectric Films," *Tokyo Sensors Product Guide Catalog*, C40J060-20120430001, pp. 1–29, 2012.
[14] D.W. Dudley, *Handbook of Practical Gear Design*. Lancaster: Technomic Publishing Company, 1994, pp. 5–119.
[15] *Japanese Industrial Standard Collection*. Tokyo: Technical and Industrial Book Company, 2015, pp. 11.11–11.17 (in Japanese).
[16] B. Suciu, K. Koyanagi, and H. Nakamura, "Evaluation of the Energy Harvestable from an Airless Tire Employing Radially Distributed Piezoelectric Spokes or Circumferentially Distributed Piezoelectric Omega Springs," *Transactions of the JSME*, 81(824), pp. 14.00560.1–14, 2015 (in Japanese).
[17] K.H. Baumgartel, D. Zollner, and K.L. Krieger, "Classification and Simulation Method for Piezoelectric PDVF Sensors," *Procedia Technology*, 26, pp. 491–498, 2016.
[18] Y. Hu, W. Kang, Y. Fang, L. Xie, L. Qiu, and T. Jin, "Piezoelectric Poly (vinylidene fluoride) (PVDF) Polymer-Based Sensor for Wrist Motion Signal Detection," *Applied Sciences*, 8(836), pp. 80.50836.1–12, 2018.
[19] P. Martins, A.C. Lopes, and S.L. Mendez, "Electroactive Phases of Poly(vinylidene fluoride). Determination, Processing, and Applications," *Progress in Polymer Science*, 39, pp. 683–706, 2014.
[20] "MR8870 Memory High-Recorder," *HIOKI Instruction Manual*, pp. 1–18, 2018.
[21] G.W. Stachowiak, and A.W. Batchelor, *Engineering Tribology*. Amsterdam: Elsevier, 2005, pp. 1–795.
[22] L.L. Howell, *Compliant Mechanisms*. New York: John Wiley & Sons, 2001, pp. 1–72.

Barenten Suciu was born on July 9, 1967. He received Dr. Eng. Degrees in the field of Mech. Eng. from the Polytechnic University of Bucharest, in 1997, and from the Kobe University, in 2003. He is working as Professor at the Department of Intelligent Mech. Eng., Fukuoka Institute of Technology. He is member of JSME, JSAE, and JSASS. His major field of study is the tribological and dynamical design of various machine elements.